Quaternary Science Reviews 378 (2026) 109874

Contents lists available at ScienceDirect

Quaternary Science Reviews

journal homepage: www.elsevier.com/locate/quascirev

Midsommersø records the Holocene glacial history of Wandel Dal, Inutoqqat Nunaat (Peary Land) northern Greenland

Nicholas L. Balascio [a,b,*], Jostein Bakke [c], Bianca Perren [d], William J. D'Andrea [e], Elizabeth Diaz [b], Francois Lapointe [f], Raymond S. Bradley [f], Redmond Stein [e], Zachary Van Dusen [a], Frederik Fuuja Larsen [g], Christian Koch Madsen [g]

[a] Department of Earth & Climate Sciences, Bates College, Lewiston, ME, USA
[b] Department of Geology, College of William & Mary, Williamsburg, VA, USA
[c] Department of Earth Science and the Bjerknes Centre for Climate Research, University of Bergen, Bergen, Norway
[d] British Antarctic Survey, Natural Environmental Research Council, Cambridge, UK
[e] Lamont-Doherty Earth Observatory of Columbia University, Palisades, NY, USA
[f] School of Earth and Sustainability, University of Massachusetts, Amherst, USA
[g] Greenland National Museum and Archives, Nuuk, Greenland

ARTICLE INFO

Handling Editor: Dr P Rioual

Keywords:
Lake sediment
Paleoclimate
Paleolimnology
Midsommer
Wandel Dal
Peary land
Greenland

ABSTRACT

Reconstructing past ice extent and climate at the margins of the Greenland Ice Sheet (GrIS) offers important insights into the sensitivity of the ice sheet and its peripheral regions to climate forcing. Wandel Dal is a valley in northern Greenland that drains the northern margin of the GrIS as well as several ice caps. The valley was also an important landscape corridor for Inuit cultures beginning in the mid-Holocene. Here we examine the Holocene deglaciation and climate history of Wandel Dal based on analysis of sediment cores from Lake Midsommer (Midsommersø). We analyzed physical sediment properties, carbon and nitrogen content, grain size, diatom assemblages, and scanning X-ray fluorescence profiles to reconstruct physical and biological changes in the lake that were influenced by variations in glacier meltwater input, snowpack melt, precipitation, and lake primary productivity over the last c. 8.2 kyr. We find evidence that meltwater input to the lake was highest from at least c. 8.2 to c. 6.5 cal ka BP, delivering highly minerogenic sediments characterized by dense clay with frequent coarse layers. At c. 6.5 cal ka BP, there was an abrupt transition to sediment that is less dense, more organic rich, and where diatoms first appear. We interpret these changes to represent a significant reduction of meltwater input due to reduced ice extent within the catchment. These conditions lasted until c. 3.9 cal ka BP when we infer a shift to colder and drier conditions based on diatom and grain size data, which suggest longer periods of ice cover and reduced runoff to the lake. These conditions persisted until c. 50 years ago when diatom diversity dramatically increased due to recent climate warming. Our results add new constraints to the climate and deglaciation history of Inutoqqat Nunaat (Peary Land) and provide context for the Paleo-Inuit settlement history of Wandel Dal.

1. Introduction

The Arctic has experienced rapid warming in recent decades with broad implications for high-latitude ecosystems and global climate (Post et al., 2009; Taylor et al., 2022). Recent warming in Greenland is of particular concern due to the impact on Greenland Ice Sheet (GrIS) melt rates, connections to regional ocean-atmosphere dynamics, and potential threshold responses (Bintanja, 2018; Ribeiro et al., 2021; Hörhold et al., 2023; Mattingly et al., 2023; Otosaka et al., 2023). In addition to the GrIS's response to ongoing warming, peripheral glaciers and ice caps have also experienced accelerated melt in recent years, with ice loss rates from 2018 to 2021 CE of 42 ± 6 Gt/yr and with the greatest mass losses in northernmost Greenland (Khan et al., 2022). Reconstructing past ice extent and climate at the margins of the GrIS allows us to assess how present conditions compare to natural variations and provides important perspectives on the sensitivity of the GrIS and peripheral

* Corresponding author. Department of Earth & Climate Sciences, Bates College, Lewiston, ME, USA.
E-mail address: nbalascio@bates.edu (N.L. Balascio).

https://doi.org/10.1016/j.quascirev.2026.109874
Received 4 October 2025; Received in revised form 7 February 2026; Accepted 8 February 2026
Available online 17 February 2026

glaciers to change (Briner et al., 2020; Carrivick et al., 2019, 2023).

The Holocene climate history of Greenland was influenced by northern latitude summer insolation, the waning of northern hemisphere ice sheets, as well as their impact on North Atlantic oceanic and atmospheric circulation (Funder et al., 2011; Briner et al., 2016; Kjær et al., 2022; Leger et al., 2024). Precession-driven insolation trends show a maximum in summer insolation in the Northern Hemisphere during the early Holocene that resulted in warmer and longer summers. This enhanced seasonality particularly affected the High Arctic. Over the course of the Holocene, a gradual decline in summer insolation led to cooler summers and a reduction in seasonality, contributing to the expansion of ice and the onset of Neoglaciation. The early Holocene was marked by the overall retreat of the GrIS following the Last Glacial Maximum in response to insolation, changing oceanographic conditions, and eustatic sea-level rise (Funder et al., 2011; Briner et al., 2016). The Holocene thermal maximum (HTM) around Greenland generally lagged the early Holocene peak in summer insolation due to the large thermal inertia imposed by the deteriorating ice sheets and glaciers, with many proxy-based records of past temperature indicating maximum warmth during the mid-Holocene, c. 9-5 cal ka BP (Briner et al., 2016). The GrIS retreated to its minimum Holocene extent sometime between c. 6.5 and 4 cal ka BP; however, at regional scales the rate and magnitude of ice margin retreat was heterogeneous, due in part to the vast area and latitudinal range spanned by the ice sheet (Leger et al., 2024). Neoglacial cooling driven by lower summer insolation during the late Holocene led to the expansion of GrIS outlet glaciers and peripheral glaciers after c. 4 cal ka BP, with some evidence for significant advances starting at c. 2.5–1.7 cal ka BP (Kjær et al., 2022).

Despite this general understanding of the Holocene glacial and climate history at the margins of the GrIS, there remain spatial and temporal data gaps. New glacial and environmental reconstructions can improve constraints on the evolution of the GrIS, peripheral glaciers, and aspects of Arctic climate history. In this study, we use sediment records from Lake Midsommer (Midsommersø) to investigate the Holocene deglaciation and climate history of Wandel Dal, a valley in *Inutoqqat Nunaat* (Peary Land), northern Greenland (Fig. 1). Midsommerø receives meltwater from the northern margin of the GrIS, as well as from the Hans Tausen, Bure, and Storm ice caps. Former ice limits have been identified in Wandel Dal in recent reconstructions, but remain undated (Leger et al., 2024) and no existing continuous paleoclimate records document past environmental changes of this High Arctic environment.

Lakes in remote polar regions offer exceptional potential for reconstructing past climate and environmental change. Their sediments accumulate continuously and are often undisturbed, preserving layered archives of physical, chemical, and biological signals that reflect both local and regional climate dynamics (e.g., Bakke et al., 2018; Adamson

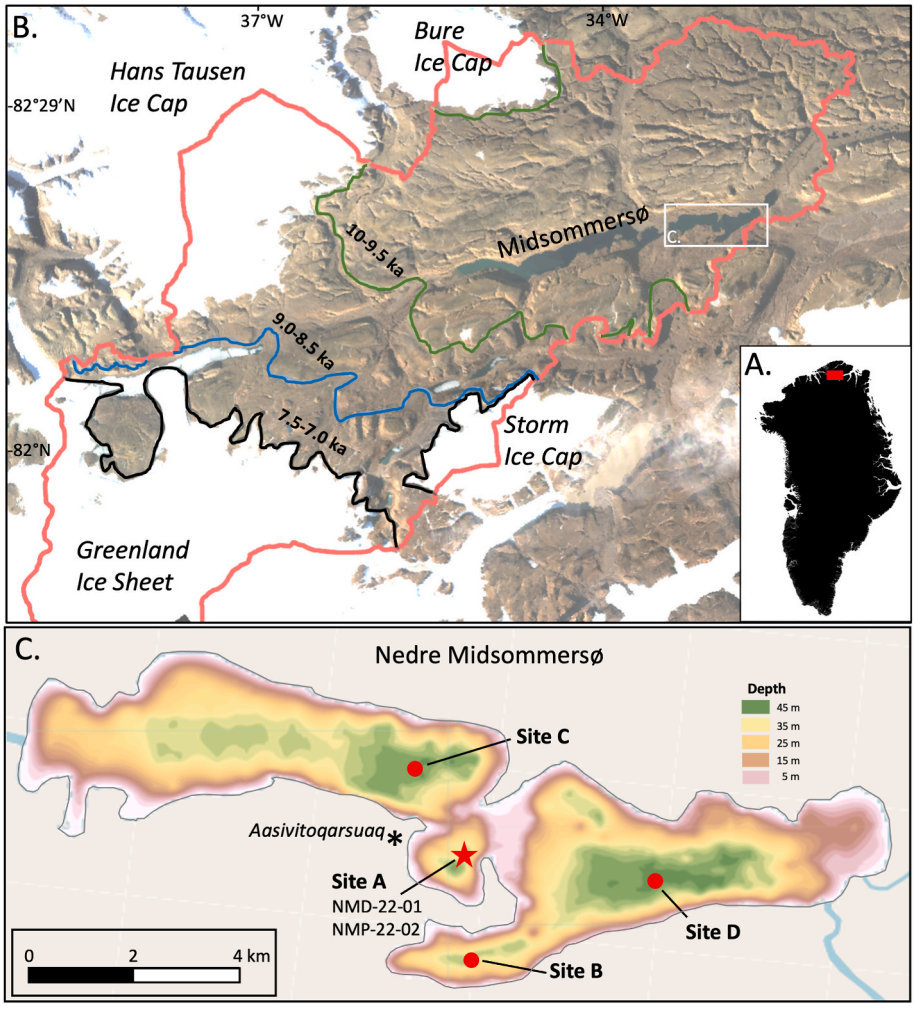

Fig. 1. (A.) Location of the study area in the High Arctic of northern Greenland. (B.) Midsommersø in the center of Wandel Dal showing the catchment area (pink line) and mapped early Holocene ice limits from Leger et al. (2024). Note that ice limits are mapped with low and very low confidence and not based on direct dating in Wandel Dal. (C.) Bathymetric map for Nedre Midsommersø showing the locations of our coring sites, including Site A cores which are the primary focus of this study (Table 1). The location of the Independence I sites of Aasivitoqarsuaq ("Pearylandville") is also indicated. (For interpretation of the references to color in this figure legend, the reader is referred to the Web version of this article.)

et al., 2022). In areas where direct evidence of past glacial extent or atmospheric conditions is limited, lake sediments serve as natural repositories of information, capturing the impacts of temperature shifts, hydrological changes, and fluctuations in ice margins. Advances in analytical techniques — such as high-resolution geochemical scanning, sedimentological modelling, and microfossil analysis — have greatly enhanced our ability to extract detailed climate records from these archives. As such, lakes represent a powerful and increasingly accessible tool for understanding long-term environmental variability in some of the most sensitive and least studied parts of the planet.

Here we present sediment core data from Nedre (Lower) Midsommersø. We characterize the physical and biological response of the basin to paleoenvironmental conditions. Our interpretations are based on the analysis of bulk density, mass accumulation rates, carbon and nitrogen content, grain size, diatom assemblages, and scanning X-ray fluorescence (XRF) profiles. We use these data to infer changes in GrIS and local glacier meltwater input, surface runoff from snowmelt and precipitation, and duration of summertime lake ice cover over the last c. 8.2 kyr, and to place these changes in the context of the climate history of northern Greenland.

2. Study area

Wandel Dal is located in the southern region of Inutoqqat Nunaat (*Land of the Ancient People*), in the High Arctic of northern Greenland (Fig. 1A). The region is a polar desert with low annual average precipitation and temperatures. The nearest weather station is at Station Nord (81°35′57”N, 16°38′12”W), located 280 km to the east on the northeast coast of Greenland. Observations at Station Nord since 1961 CE indicate mean annual temperatures of −16 °C and mean annual precipitation of 258 mm, however Wandel Dal experiences colder and dryer conditions due to its continentality. Station Nord data also show a ~3 °C increase in mean annual temperatures since 1961 and a ~200 mm increase in mean annual precipitation, which reflects the sensitivity of this region to recent global warming.

Wandel Dal is a west-east trending U-shaped valley that connects J.P. Koch Fjord to the west with Jørgen Brønlund Fjord, a tributary of Independence Fjord, to the east. The valley separates the GrIS and Storm Ice Cap to the south from the Hans Tausen and Bure Ice Cap to the north (Fig. 1B). During the early Holocene, the GrIS merged with the local ice caps and occupied the valley. Former ice positions and a regional compilation of ages extrapolated from nearby regions have been used to estimate that ice retreated out of Midsommersø c. 10-9.5 cal ka BP and that the GrIS margin and local ice caps may have been near their present margins by c. 7.5-7.0 cal ka BP (Fig. 1B; Leger et al., 2024). However, there are no directly dated moraines in Wandel Dal, and ice positions are mapped with “low” and “very low confidence” (Leger et al., 2024).

Midsommersø (82° 15′ N, 34° 15′ W; 180 m a.s.l.) is positioned in the center of Wandel Dal and consists of two basins: Øvre (*upper*) Midsommersø and Nedre (*lower*) Midsommersø (Fig. 1B). The lake is above the local marine limit, which is mapped at 65 m a.s.l. based on data 50 km to the east in the Jørgen Brønlund Fjord area (Bennike, 1987; Landvik et al., 2001). Øvre Midsommersø has a surface area of ~58 km^2 and Nedre Midsommersø has a surface area of ~26 km^2 and a maximum water depth of 45 m. The two lakes are separated by a large fan delta built out from the valley draining the north and are connected by a 1-km long and 0.07-km wide, shallow channel (<3 m depth). The bathymetry of Nedre Midsommersø shows that the lake consists of four distinct 40-45 m deep basins (Fig. 1C). The lakes have a combined catchment area of 5400 km^2 and receive meltwater from sectors of the Greenland Ice Sheet, and the Hans Tausen, Bure, and Storm Ice Caps (Fig. 1). The valley walls around the lake reach elevations of ~700-800 m immediately north and south of the lakes.

Bedrock around Midsommersø is primarily Mesoproterozoic to Cambrian sedimentary rocks (Pedersen et al., 2013). The Inuiteq Sø, Portfjeld and Buen Formations underlie the southern and western portions of the catchment. The Mesoproterozoic Inuiteq Sø Formation is a feldspathic to quartzitic, medium to coarse-grained sandstone. Dolerite intrusions are found throughout this formation, including areas around the margins of Midsømmersø. The Portfjeld Formation is Neoproterozoic dolomite and stromatolitic dolomite with some sandstone intervals. The Cambrian Buen Formation consists of sequences of quartzitic sandstone that grade into shale, interbedded with greywacke. The northern portion of the catchment also drains areas underlain by Cambrian and Ordovician dolomites of the Brønlund Fjord Formation, the Wandel Valley Formation, and the Børglum River Formation.

Wandel Dal has been an important corridor for human migration and occupation since c. 4.5 cal ka BP (Knuth, 1967a, 1967b; Grønnow and Jensen, 2003; Jensen et al., 2017; Jensen and Gotfredsen, 2022). Numerous archaeological sites have been identified in Wandel Dal and along the shores of Midsommerø associated with the Independence I (c. 4.5-3.9 cal ka BP), Greenlandic Dorset (c. 2.8-2.4 cal ka BP), and Thule (c. 1400 CE) cultures (Grønnow and Jensen, 2003). These sites include *Aasivitoqarsuaq* (*The Gathering Place*) formerly called “Pearylandville” (Knuth, 1967a, 1967b) (Fig. 1C). Aasivitoqarsuaq is the largest known summer settlement, and perhaps even a gathering site, of the Independence I people located along the southern shore of Nedre Midsommersø.

3. Methods

3.1. Sediment core collection and analysis

Sediment cores were recovered from a floating platform at four sites (A, B, C, D) within the main basins of Nedre Midsommersø in August 2022 (Fig. 1C). Two cores were collected at each site – a short gravity core (NMD) to recover an intact sediment-water interface and a longer piston core (NMP) (Table 1). Scanning XRF profiles and visual stratigraphic changes were used to align NMD and NMP cores to create composite stratigraphies for each site, which range in length from 504.9 to 577.2 cm. We focused on developing an age-depth model and sedimentological reconstruction based on analysis of the sediment cores from site A (NMD-22-01, NMP-22-02), which is closest to the main Independence I archaeological site at Aasivitoqarsuaq (Fig. 1C). However, visual lithostratigraphy, bulk density data (calculated as the mass of 1 cm^3 samples after freeze drying), and select scanning XRF profiles from all four composite records were used to assess basin-wide sediment characteristics.

3.2. Age-depth modeling

An age-depth model for the composite record from Site A was established based on radiocarbon measurements and analysis of anthropogenic cesium (^{137}Cs). Radiocarbon dating was performed on thirteen plant material samples isolated from NMD-22-01 and NMP-22-02 (Table 2). Plant material was isolated by washing samples in deionized water over a 125 μm sieve and isolating plant fragments using a binocular microscope. The plant material recovered was too small for identification. Samples were analyzed at the University of California, Irvine Keck Carbon Cycle AMS Laboratory. Radiocarbon dates were calibrated using the IntCal20 calibration dataset (Reimer et al., 2020).

The activity of ^{137}Cs in the upper 3 cm of the gravity core (NMD-22-01) was measured to confirm the recovery of an intact sediment-water interface. Radioactive cesium is present in lake sediment from atmospheric nuclear weapons testing fallout that became significant in 1952 CE and peaked from 1963 to 1964 CE (Ritchie and McHenry, 1990; Beck and Bennett, 2002). ^{137}Cs activity was measured by ultra-low background gamma spectrometry in the Department of Geology at the College of William & Mary. Samples were taken every 0.5 cm and freeze-dried, ground, and packed into 2-cm diameter containers. They were then analyzed on a heavily shielded Canberra Broad Energy (BE5030) intrinsic germanium detector for 2-6 days. An age-depth model was generated based on all of the chronologic information

Table 1
Nedre Midsommerø sediment core sites and core information (Fig. 1C).

Coring Site	Latitude (°N)	Longitude (°W)	Core Name	Coring Method	Sediment length (cm)	Composite Length (cm)
A	82.225369	33.423935	NMD-22-01	gravity	172	558.6
			NMP-22-02	piston	514.5	
B	82.210516	33.410184	NMD-22-02	gravity	109	545
			NMP-22-03	piston	539	
C	82.238842	33.448944	NMD-22-03	gravity	132.5	504.9
			NMP-22-04	piston	500.5	
D	82.222612	33.270697	NMD-22-04	gravity	130	577.2
			NMP-22-05	piston	554.5	

Table 2
Radiocarbon sample information for Nedre Midsommersø cores NMD-22-01 and NMP-22-02.

Laboratory IDa	Composite Depth (cm)	Sample Name	Material Dated	Radiocarbon Age (yr BP, ±)		Calibrated Age Range (yr BP, 2σ)	Median Age (cal yr BP)
UCIAMS-282424	33	NMD-22-01	Plant material	1785	20	1613-1722	1656
UCIAMS-282426	67	NMD-22-01	Plant material	2660	20	2744-2842	2763
UCIAMS-278327	71.4	NMP-22-02 1/4	Plant material	3340	90	3385-3828	3576
UCIAMS-282425	96	NMD-22-01	Plant material	3920	20	4256-4419	4359
UCIAMS-278328	101.4	NMP-22-02 1/4	Plant material	3645	15	3898-4075	3954
UCIAMS-278322	136.9	NMP-22-02 1/4	Plant material	7880	25	8592-8853	8667
UCIAMS-278329	166.4	NMP-22-02 1/4	Plant material	4505	20	5050-5295	5156
UCIAMS-278324	191.4	NMP-22-02 2/4	Plant material	4595	25	5141-5445	5317
UCIAMS-278323	218.4	NMP-22-02 2/4	Plant material	5025	25	5660-5895	5814
UCIAMS-278326	252.4	NMP-22-02 2/4	Plant material	5270	90	5769-6283	6064
UCIAMS-278321	276.4	NMP-22-02 2/4	Plant material	8550	35	9484-9547	9528
UCIAMS-278325	302.4	NMP-22-02 2/4	Plant material	6090	70	6786-7161	6959
UCIAMS-278330	514.9	NMP-22-02 4/4	Plant material	6880	15	7667-7777	7701

aUCIAMS - University of California Irvine Keck-CCAMS Facility.

using the Bacon age-modelling software in R (Blaauw and Christen, 2011). Unless otherwise indicated, all ages are reported in calibrated thousand year before present (cal ka BP), with present fixed at 1950 CE by convention.

3.3. Thin-section analysis

Sediment thin sections were made from select locations within NMP-22-02 to characterize sediment texture and structure. A total of 21 metal trays, each 19 cm in length and filled with sediment extracted from the cores (Francus and Asikainen, 2001), were flash frozen through gradual immersion in liquid nitrogen and subsequently freeze-dried (Lapointe et al., 2019). Following drying, the sediment within the trays was embedded in epoxy resin using the method described by Lamoureux (1994). Sixty-three overlapping thin sections were prepared, each exposing approximately 5 cm × 2 cm of sediment, to cover the upper laminated sequences of the record. These thin sections were then digitized using a high-resolution flatbed scanner at 2400 dpi, yielding an image resolution of 10.6 μm per pixel. We present a selection of results from this analysis to highlight characteristics of the lithostratigraphy observed in thin section.

3.4. Scanning X-ray fluorescence (XRF)

Sedimentary elemental abundances were characterized at high resolution using an Itrax™ X-ray fluorescence (XRF) core scanner (Croudace et al., 2006). The Itrax nondestructively scans the sediment surface and outputs elemental compositions as peak areas from dispersive energy spectrum, which reflect their relative concentrations. Elemental changes can be related to the source and composition of lithogenic sediments, as well as post-depositional geochemical reactions.

Measurements were made in EARTHLAB at the Department of Earth Science at the University of Bergen. Split core surfaces were scanned at 200 or 500 μm intervals with an exposure time of 10 s. Elemental data are presented relative to the total counts per second. Overall count rates are low for most elements with the exception of silicon (Si), potassium (K), calcium (Ca), titanium (Ti), and iron (Fe). We attribute the overall low count rates to the sedimentary bedrock within the catchment. We focused our analysis on Si, K, Ca, Ti, and Fe, and examined trends among them using correlations and principal component analysis.

3.5. Bulk organic matter

Total carbon and nitrogen content of samples was measured to identify the amount and composition of organic matter throughout NMP-22-02 and NMD-22-01. Inorganic carbon was not present in significant concentrations, as determined by acid fumigation testing. Changes in organic carbon concentration can be attributed to the flux of minerogenic material entering the lake, the flux of terrestrial organic matter entering the lake, changes in aquatic primary productivity (e.g. driven by nutrient availability, lake water temperature, and/or ice cover conditions), and changes in the preservation of organic matter (Meyers, 2003). The ratio of organic carbon to total nitrogen (C/N) can reflect the relative proportion of allochthonous versus autochthonous organic matter (Meyers, 2003). C/N values between 4 and 10 are typical of algae, while values greater than 10 suggest contributions from terrestrial plants (Meyers, 2003).

An Elementar vario MICRO cube elemental analyzer was used to measure the total carbon and total nitrogen concentration on selected samples. Samples were freeze-dried, ground, and approximately 8-15 mg were weighed into tin capsules. Calibration curves were generated for each run using six sulfanilamide standards with a range of masses. Uncertainties in weight percent nitrogen and carbon values are 0.03% and 0.4%, respectively, based on the average standard deviation of triplicate analyses. C/N values were calculated as the molar ratio of total organic carbon to total nitrogen. Additional measurements from each core section were made on select samples (n = 20) from each core section that were acid fumigated (Harris et al., 2001) prior to analysis to test for the presence of inorganic carbon. These samples were weighed

into silver capsules, wetted with deionized water, and placed in a desiccator with a beaker of concentrated hydrochloric acid. After 8 h, the samples were removed from the desiccator, dried at 50 °C, and then folded into tin capsules for analysis. In all instances, the difference between carbon values for unacidified and acidified samples was smaller than the analytical uncertainty for weight percent carbon (0.4%), with a mean difference of 0.08%.

3.6. Diatom analysis

Diatom assemblages were identified in select samples from cores NMP-22-02 and NMD-22-01 to assess aquatic water column conditions and aquatic productivity throughout the record. Diatoms were isolated from wet sediment (0.3 g) following standard oxidative procedures for large sample numbers (modified from Renberg, 1990). Diatom slurries were mounted on plain glass coverslips using Naphrax mounting medium and identified at 1000x using light microscopy. At least 400 valves were identified per slide. Taxonomy followed reference literature, principally Antoniades et al. (2008), as well as other regional references (e.g. for Inutoqqat Nunaat: Foged, 1955). Additionally, chrysophyte cysts were enumerated but not identified. Given the limited species diversity and overturn, compositional changes were evaluated using Principal Component Analysis (PCA) on diatom relative species abundances. PC axes 1 and 2 describe 58% and 23% of the diatom compositional change respectively. Effective species diversity was calculated as Hill's N2.

3.7. Grain size analysis

Grain size data were collected to understand changes in the delivery of lithogenic sediment to the lake. Grain size analysis was performed on 99 samples taken from throughout NMP-22-02 and NMD-22-01. Samples were pretreated with 10 ml of 10% hydrogen peroxide for 48 h to remove organic matter, and for 24 h with 20 ml of sodium hexametaphosphate to disaggregate particles before analysis on a Beckman Coulter LS13320 laser diffraction particle size analyzer with an Aqueous Liquid Module. Samples were sonicated prior to and during analysis to prevent particle flocculation and were run in triplicate. Volume percentages of 92 size classes (0.375-2000 μm) were measured, results from the triplicate runs were averaged, and the percent composition of sand (2000-63 μm), silt (63-4 μm), and clay (<4 μm), and the mean grain size were determined for each sample.

End-member modeling was applied to further evaluate the grain size data. End-member mixing analysis (EMMA) assumes datasets represent a mixture of signals that reflect different proportional contributions of a number of subpopulations (Weltje, 1997). EMMA has been applied to decompose grain size distribution data to quantify subpopulations related to different sediment sources or transport processes within a sedimentary environment (e.g. Dietze et al., 2012; Paterson and Heslop, 2015; Macumber et al., 2018). End-member modeling was performed on our grain size dataset using the R package EMMAgeo (version 0.9.7), which is an algorithm based on principal component analysis, eigenvector rotation, and nonnegative least-square estimation (Dietze et al., 2012; Dietze and Dietze, 2019). The number of end members was determined by evaluating the cumulative variance of the potential end-members (eigenvalues). End-members are described based on their loadings and scores. Loadings quantify the relative contribution of a grain size class to each end-member (i.e. the grain size distribution represented by an end-member). Scores quantify the relative contribution of an end-member to each sample (i.e. the dominant grain size distribution within the time interval represented by the sample).

4. Results

4.1. Lithostratigraphy

The 559-cm composite record from Nedre Midsommersø Site A contains three primary lithostratigraphic units (Fig. 2). Unit I (559-311 cm) consists of a finely laminated, reddish-brown clay with numerous, thin (<2 mm) coarser layers that are darker in color. Some of these very fine sand layers contain bright particles observable in thin-section (Fig. 3i). The lowermost 20 cm contains several lenses of coarse sand, including one that is 4 cm thick. A 0.5-cm-thick moss layer at 515 cm is also present in this unit and provided the lowermost radiocarbon sample (Table 2). Unit I is dense throughout, with an average dry bulk density of 0.78 g/cm^3. The transition to Unit II (311-95 cm) is marked by an abrupt change to sediment that is less dense (average = 0.47 g cm^{-3}), finer, and darker in color (Fig. 2). Thick successive layers (interpreted as debris flows) totaling ~4 cm occur at ~280 cm (Fig. 3h), but in general, thin (<1-4 mm) laminations are present throughout and range in color from light reddish-brown to dark brown and black (Fig. 3c-g). In Unit III (95-0 cm) there is a sharp transition to sediment that is light brown in color, less dense (average = 0.27 g cm^{-3}), and with faint laminations (Fig. 2) as observed in the thin section (Fig. 3a,b). Coarse grains are sparsely distributed throughout this unit and can be visually identified (Fig. 3b).

4.2. Age-depth model

The age-depth model for the Site A sediment record is based on radiocarbon ages and Cs data (Table 2; Fig. 2). Radiocarbon results from 11 of the 13 samples exhibit a coherent pattern of increasing age with depth, with the lowermost sample at 515.5 cm having an age of 7.7 cal ka BP (Fig. 2). The samples at 136.9 cm and 276.4 cm are significantly older (2.6-3.5 cal ka BP) than adjacent samples. These anomalously old ages likely indicate reworking of old plant material, but we cannot rule out the potential influence of a hardwater effect due to the presence of dolomitic bedrock in the catchment if the samples contained some aquatic plant material that we were unable to identify. Cesium data show a value of 21.8 Bq/kg at the top of the record, with a sharp peak of 66.7 Bq/kg at 1.75 cm, declining to 2.8 Bq/kg at 3 cm. We correlated the peak in ^{137}Cs activity at 1.75 cm to the peak in atmospheric nuclear weapons testing fallout in 1963 CE, and the top of the record was assigned an age based on the year of core collection (2022 CE). All of the chronological data, excluding the old radiocarbon ages at 136.9 cm and 276.4 cm, were input into the Bacon age-modelling software in R to generate an age-depth model (Blauuw and Christen, 2011) (Fig. 2). Sedimentation rates (cm yr^{-1}) are derived from the Bacon age model and are presented as 10-cm running means (Fig. 2). The certainty of sedimentation rates below ~300 cm is much lower due to the presence of only two radiocarbon ages; consequently, we only rely on the average across this entire interval (Unit I) for interpreting depositional conditions.

The age-depth model defines the age ranges of lithostratigraphic Unit I (8.2-6.5 cal ka BP), Unit II (6.5-3.9 cal ka BP), and Unit III (3.9 cal ka BP-present). The age-depth model indicates that changes in sedimentation rate and mass accumulation rate further define lithostratigraphic units (Fig. 2). Average sedimentation rate is 0.15 cm yr^{-1} in Unit I and average mass accumulation rate is the highest of the record (0.12 g cm^{-1} yr^{-1}). The linear sedimentation rate starts to decline in Unit II and decreases from ~0.15 to 0.05 cm yr^{-1} across Unit II. Average mass accumulation rate in Unit II is 0.04 g cm^{-1} yr^{-1}. The transition to Unit III is marked by a sharp decrease in linear sedimentation rate to 0.03 cm yr^{-1}, which is also the average across this unit. Average mass accumulation rate is in Unit III is also the lowest of the record (0.01 g cm^{-1} yr^{-1}).

4.3. Scanning XRF analysis

XRF elemental profiles of Si, K, Ti, Ca, and Fe display variations that

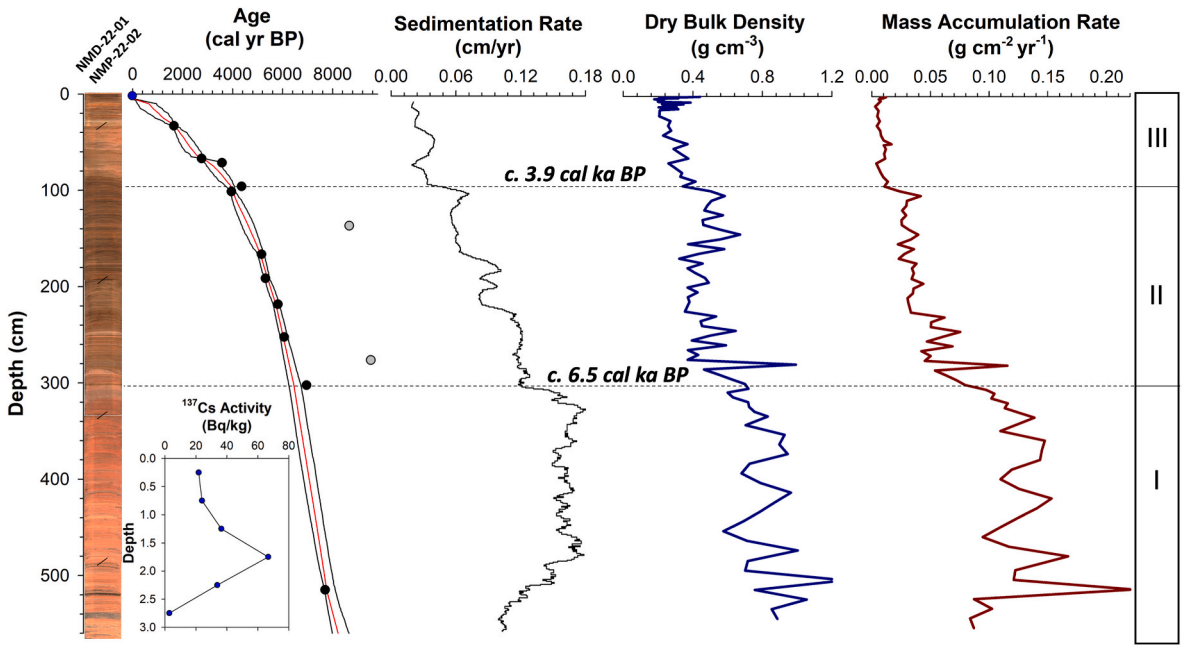

Fig. 2. Stratigraphic data for cores NMD-22-01 and NMP-22-02, including core photographs, chronologic data, sedimentation rates (10-cm running mean), bulk density, and mass accumulation rates. The positions of the three stratigraphic units (I, II, III) and the timing of the transitions is indicated with horizontal dashed lines.

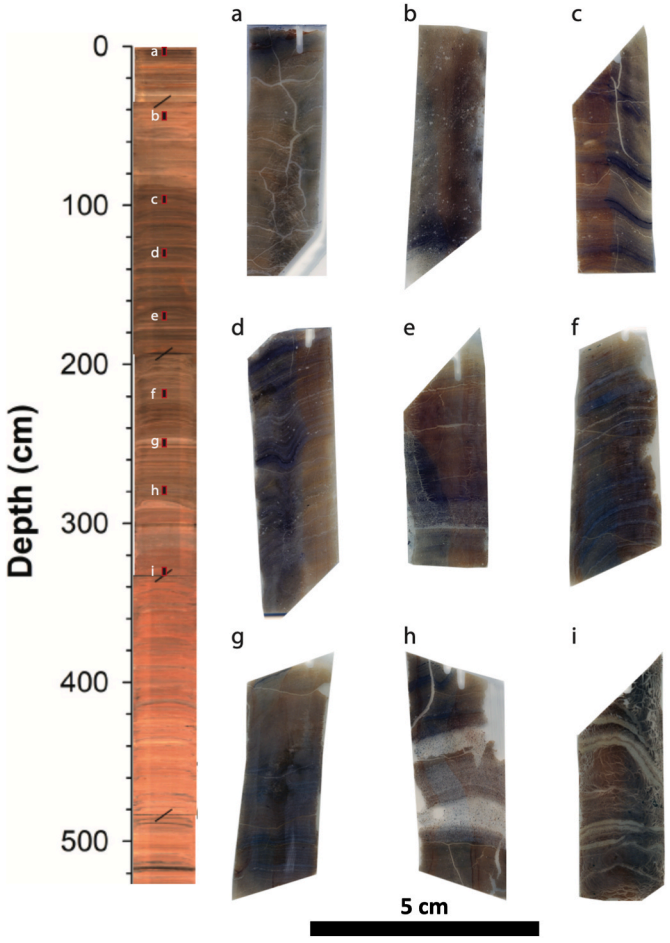

Fig. 3. Images of select thin sections from core NMP-22-02 showing characteristic sediment texture and structures.

correspond to the three main lithostratigraphic units (Fig. 4). Pearson correlations show the most significant relationships among Si, K, and Ti ($R > 0.8$). Ca and Fe are less strongly correlated to the other elements. PCA of the scanning XRF data show the first two principal components (PC1, PC2) represent 88% of the variability (Fig. 5). PC1 accounts for 67% of the variance and is primarily explained by Si, K, and Ti, which have similar loadings of 0.52, 0.52, and 0.48, respectively (Fig. 5). Fe and Ca are poorly correlated ($R = -0.01$), but explain most of the variance of PC2 with loadings of −0.68 and 0.70, respectively (Fig. 5). Ca values show the most distinct changes in variability across the three lithostratigraphic units.

Profiles of K, Fe, and Ca reflect these primary trends in the record from Nedre Midsommersø (Fig. 4). Fe and Ca profiles have their highest values and have the greatest variability in Unit I. K exhibits a decreasing trend across Unit I. Across Unit II, K values continue to decline, Ca values show an abrupt shift toward lower average values, and Fe shows a slight declining trend. The transition to Unit III is marked by a shift toward lower values and less variability in all element profiles, however the transition in Ca values is the most pronounced. Profiles of PC1 closely follow the trends in K, and PC2 most closely follows trends in Ca.

4.4. Grain size data

The average grain size composition of the record is 9% sand, 47% silt, and 44% clay. Unit I has the coarsest average grain size and exhibits the most variable grain size (Fig. 6). The mean grain size of Unit I is 27 μm, with a range of 2 μm to 170 μm. There is an abrupt change to finer sediment that marks the transition to Unit II. Across Units II and III, there is little change in average grain size, although the percentage of silt and clay shows a marked shift from average values of 59% and 37%, respectively, in Unit II to 44% and 47%, respectively, in Unit III.

Results of the EMMA show that a model with three end-members best represents our dataset and explains 95% of the variance (Fig. 7). The first end-member (EM1) has a mode of 0.7 μm with a distribution dominated by clay and very fine silt, which represent 80% of the composition. The second end-member (EM2) has a mode of 7.4 μm with 66% of the distribution within the silt size range. The third end-member (EM3) has a mode of 92 μm with 65% of the distribution within the

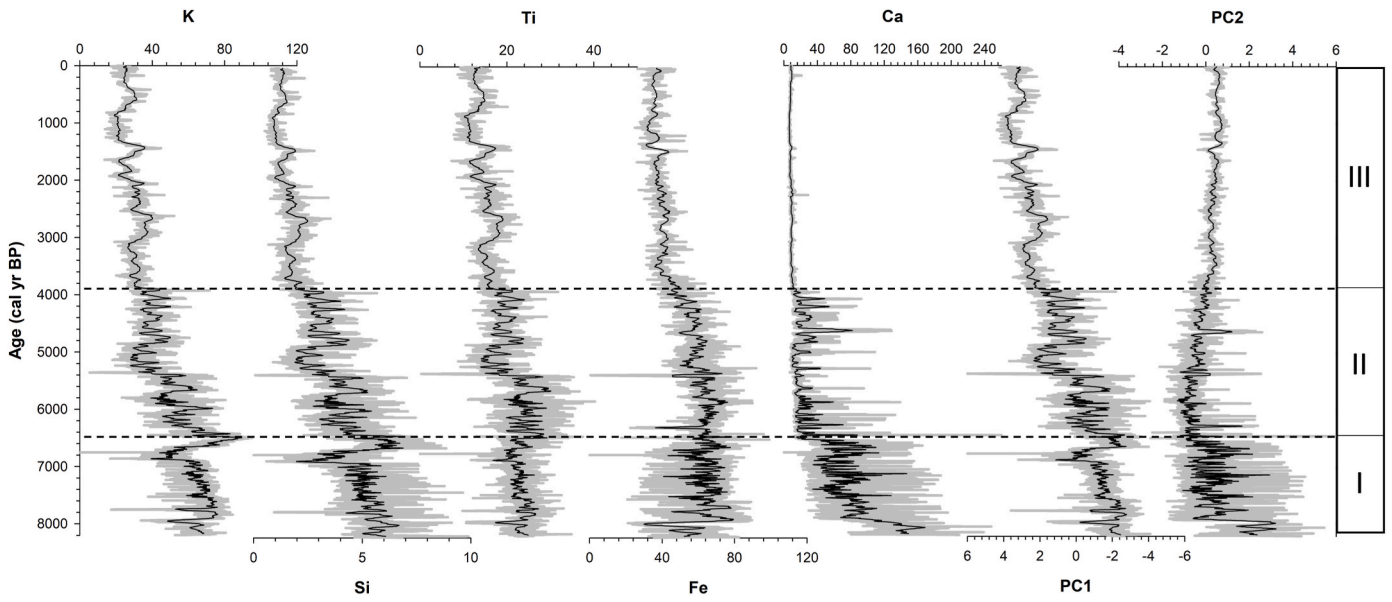

Fig. 4. Scanning XRF data for cores NMD-22-01 and NMP-22-02 showing profiles for Si, Ti, K, Fe, and Ca. All elements are presented relative to total counts per second. Principal component analysis of the entire dataset was conducted and profiles are shown of the first two principal components (PC1, PC2) (Fig. 4). Gray line represent individual measurements and black lines are 100-point running means.

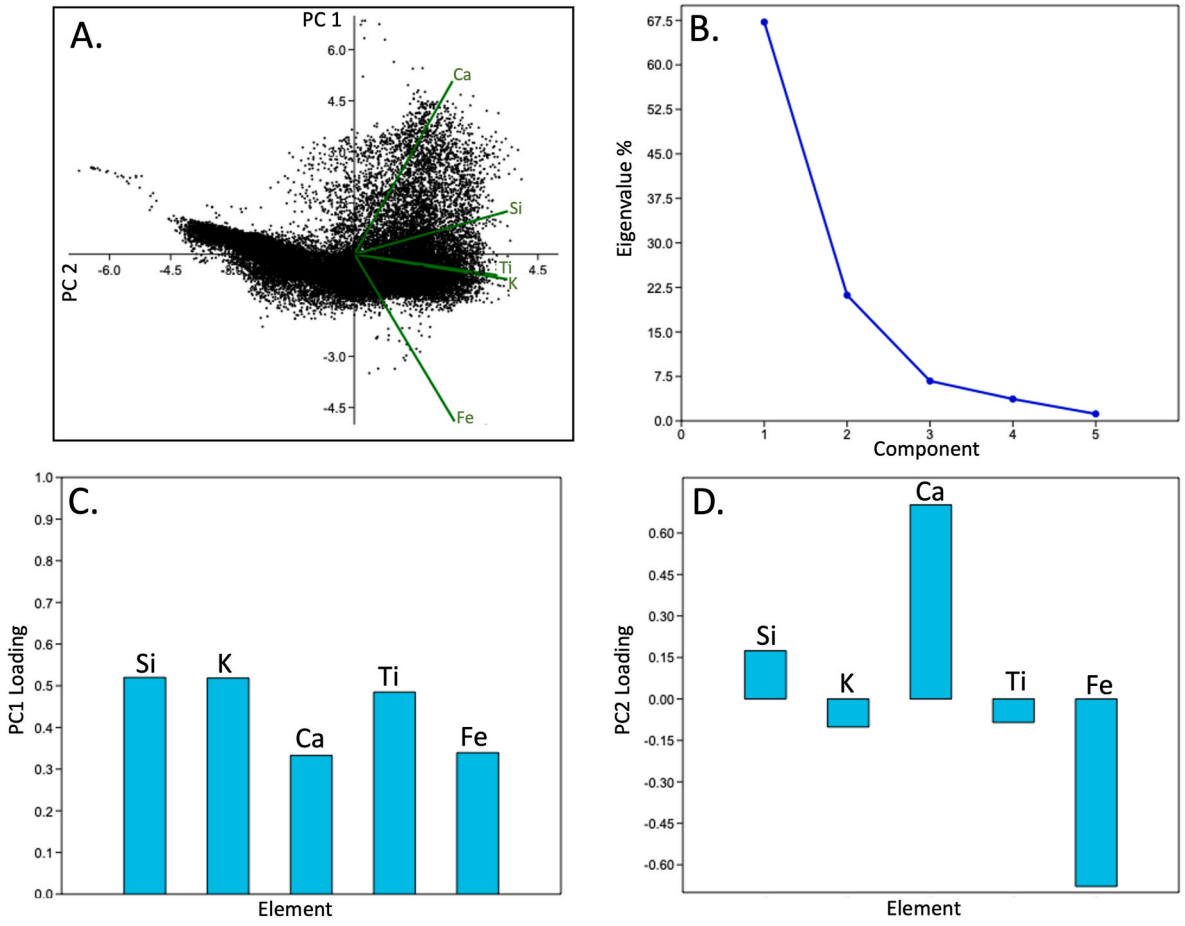

Fig. 5. Results of the principal component analysis of the scanning XRF elemental dataset for cores NMD-22-01 and NMP-22-02, including PC1 and PC2 scores and eigenvectors (A.), eigenvalue percentages for each component (B.), loadings for PC1 (C.), and loadings for PC2 (D.).

coarse silt to sand size range.

The EMMA defines grain size distributions associated with each lithostratigraphic unit as discrete end members (Fig. 7). We assess how much of the variability an end-member represents within each Unit

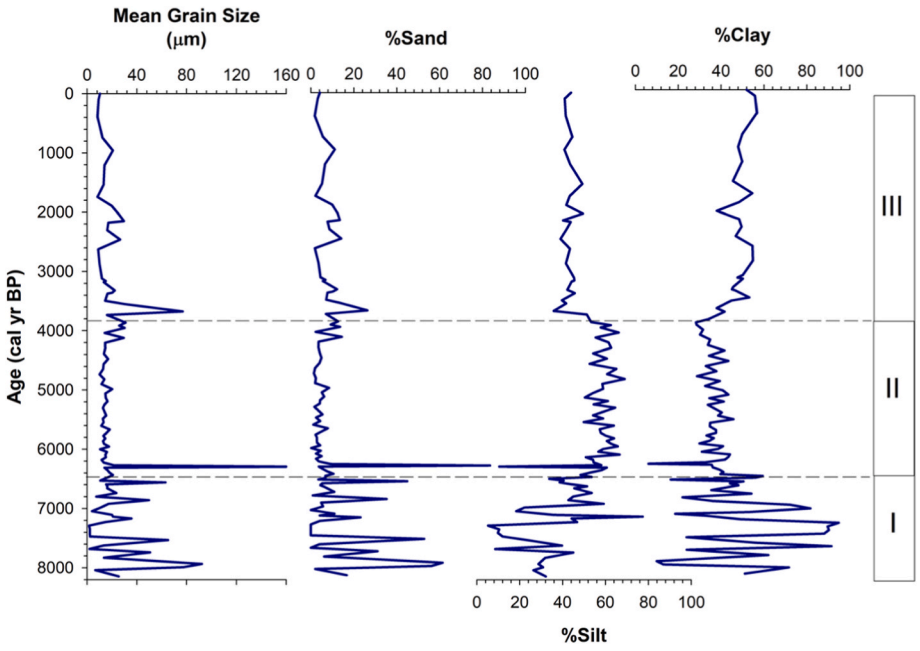

Fig. 6. Grain size data for cores NMD-22-01 and NMP-22-02, including profiles of mean grain size, %sand, %silt, and %clay.

based on their average scores. In Unit I, grain size distributions are bimodal and represented primarily by EM1 and EM3, which represent 45% and 32% of the variability of grain size distributions within this interval. The transition into Unit II is marked by an abrupt shift to grain size that is distinctly unimodal and is represented by EM2, which represents 78% of the variability. Grain size distributions similar to EM1 and EM3 within Unit II are minor at only 15% and 1%, respectively. Unit III is marked by a change to slightly finer sediment that is best represented by EM2, which represents 61% of the variability. EM3's contribution is less than 1% to the distributions in Unit III, however EM2 does contribute 38%.

4.5. Organic matter

Organic matter properties show minor variations that correspond to unit boundaries (Fig. 8). Average percent carbon values for the entire record are 2.4%. Values are generally lowest in Unit I, averaging 1.4%, and show a slight shift to higher average values in Unit II (2.4%). Values increase across Unit III and reach 6% near the top of the record, at 0.05 cal ka BP (1900 CE). C/N values average 6 across the entire record indicating that organic matter is dominated by algal sources. They are highly variable in Unit I, with a range from 1.6 to 14. C/N values are more stable across Units II and I with an average of 5.8 and only slight changes across the unit boundary.

4.6. Diatoms

Diatoms are absent from the sediments until 6.5 cal ka BP, whereupon pioneering taxa become established (Fig. 8). These consist of small, benthic Fragilariaceae (e.g. *Staurosirella* spp., *Pseudostaurosira* spp., *Staurosira* spp.) as well as large, deep-dwelling *Campylodiscus* sp. which are common to postglacial sequences at lower latitudes as well as large, deep, ice-covered lakes in the High Arctic (e.g. Sawtooth Lake, Perren et al., 2003; Lower Murray Lake, Besonen et al., 2008). Their persistence over the last 6500 years suggests a low-light, ice-dominated lake until the last ~50 years when greater species diversity of non-Fragilarioid taxa (e.g. Naviculoid and Cyclotelloid species) and habitats (e.g. epiphytic, planktonic, etc.) became established. Changes since 1980 CE are consistent with the dramatic response of circumarctic diatom communities to recent climate warming and the increase in ice-free summer days over the last several decades (Smol et al., 2005). They echo the timing of shifts in diatom communities seen in other locations in northernmost Greenland (Perren et al., 2012).

4.7. Basin-wide lithostratigraphy

Basin-wide sedimentation was characterized by comparing visual lithostratigraphy and scanning XRF Ca profiles among all four composite records from Sites A, B, C, and D (Fig. 9). The lowermost sediment unit recovered from all of the sedimentary basins in Nedre Midsommersø is dense, organic poor and clay-rich, and transitions to a darker, less dense sedimentary unit with distinct laminations. This change in properties is also reflected in Ca profiles that show higher values in the lower sediments, and the transition is defined by a distinct drop in values (Fig. 9). This transition corresponds to the change from Unit I to Unit II, characterized in detail for Site A (Figs. 2–8). However, the sediment thicknesses of the units, and the depth and thickness of the transitions vary among the sites. The transition spans approximately 5-20 cm in records from Site A, B, and C, and spans almost 50 cm as Site D. The depth of this transition is similar in records from Site A and B (c. 310 cm), and shallower at Site C (c. 110 cm) and Site D (c. 205) reflecting different sedimentation rates at each location within the basin.

5. Discussion

Characteristics of sedimentation in Midsommersø reveal three distinct phases that reflect the deglaciation and aspects of the Holocene climate history of Wandel Dal. We interpret physical and biological changes in the lake as indicators of variations in glacier meltwater input, snowpack melt, and precipitation, and lake primary productivity. We infer that these conditions were in response to early Holocene ice retreat, reduced ice extent during the mid-Holocene, and late Holocene Neoglacial conditions. Midsommersø sediments appear to document these local climate intervals, characterized by abrupt sedimentological transitions in response to changes in environmental conditions.

Our sediment record from Midsommersø extends into the early Holocene, c. 8.2 cal ka BP, which is generally a period marked by GrIS retreat, aside from a few short-lived intervals where the ice sheet deposited moraines (Briner et al., 2016). Climate of the early Holocene is defined by higher summer insolation values, average summer

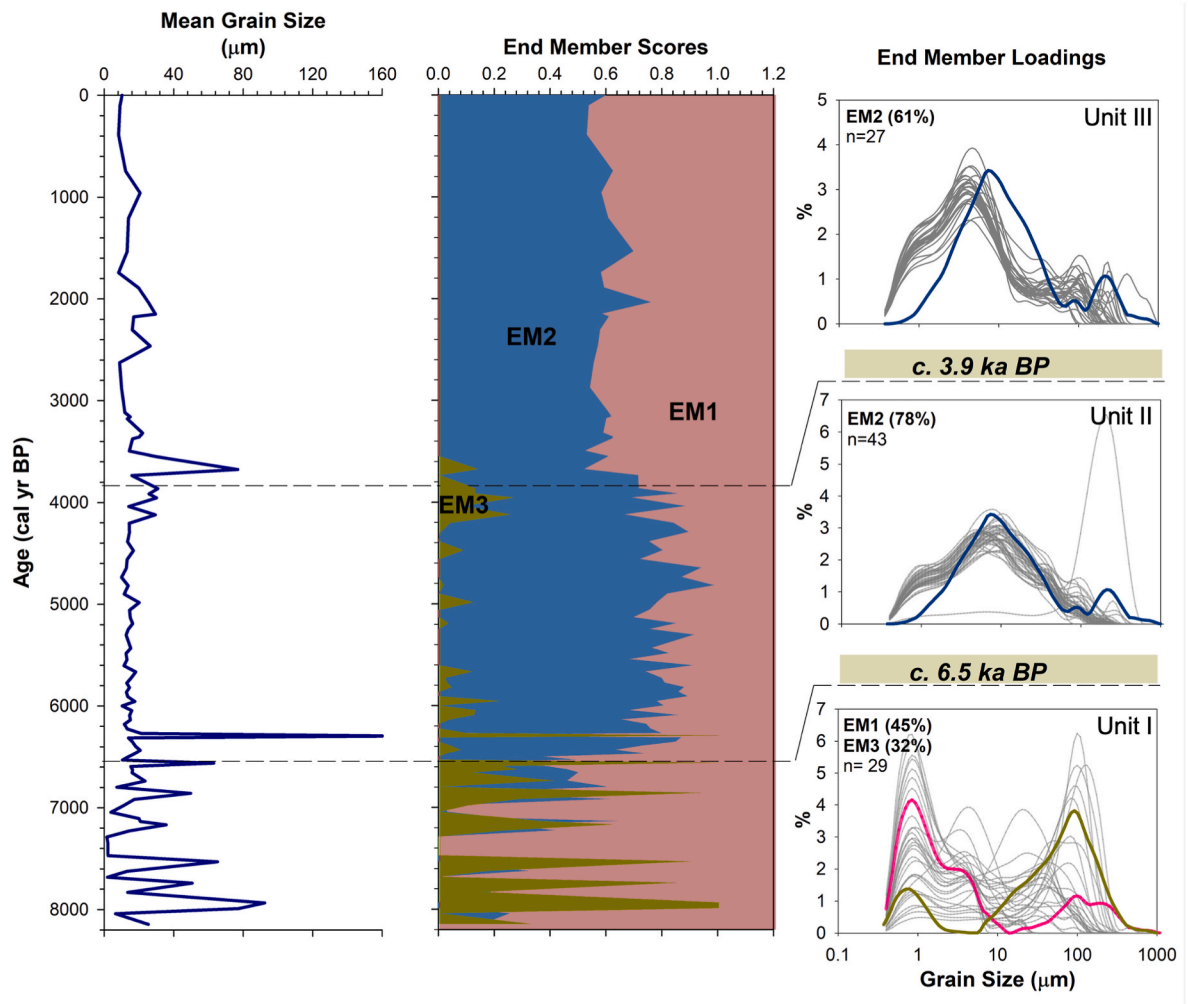

Fig. 7. Results from end-member modeling analysis of the grain size dataset compared with trends in mean grain size (Left). Down core trends in scores for the first end-member (EM1), second end-member (EM2), and third end-member (EM3) are shown with an area plot (Middle). For each lithostratigraphic unit, we also show the primary end-member loading(s) (colored lines), the average percentage score for the end-member, and the individual grain size distributions measured (gray lines) (Right).

temperatures around Greenland of at least 3-4 °C above present, and warmer ocean conditions in nearby Fram Strait (Laskar et al., 2004; Müller et al., 2012; Werner et al., 2013; Werner et al., 2016; Buizert et al., 2018) (Fig. 10). Characteristics of sedimentation in Nedre Midsommersø provide additional context for the deglaciation of Wandel Dal and ice retreat in northern Greenland. Deglaciation of Independence Fjord and areas to the east have been assessed based on cosmogenic surface exposure ages and compiled radiocarbon dates from the region (Larsen et al., 2020). These data indicate ice retreat from the outer coastal areas by c. 11 cal ka BP or earlier, followed by rapid retreat up fjord systems c. 11-10 cal ka BP. Land-based ice retreated more slowly, with some ice margins not reaching their present extent until c. 6.7 cal ka BP (Larsen et al., 2020). The head of Jørgen Brønlund Fjord is estimated to have deglaciated c. 10.2 cal ka BP, after which ice retreated up into Wandel Dal and adjacent valleys (Bennike and Björk, 2002; Larsen et al., 2020). The absolute ages of former ice margin positions have not been directly constrained at sites in Wandel Dal; however, regional mapping of ice limits that have been extrapolated through Wandel Dal provide some estimates (Leger et al., 2024). These mapped limits indicate ice may have coalesced at a position immediately above Øvre Midsommersø c. 10-9.5 cal ka BP followed by the separation of the Hans Tausen Ice Cap from the GrIS c. 9-8.5 cal ka BP, and with ice margins near their present extent c. 7.5-7.0 cal ka BP (Fig. 1.).

5.1. *Deglaciation of the western portion of Wandel Dal: c. 8.2 – 6.5 cal ka BP*

Early Holocene sedimentation in Nedre Midsommersø (Unit I; c. 8.2-6.5 cal ka BP) is characterized by dense, minerogenic sediment with relatively high sedimentation rate and an absence of diatoms (Figs. 2 and 8). Elemental abundances determined by scanning XRF display their highest values within this interval, with Ca counts being most distinctly elevated relative to subsequent intervals (Fig. 4). The large Ca signal and high amplitude variability in Unit I likely reflects the presence of Ca in the local bedrock and coarser sediment layers within this unit. Unit I is defined by a bimodal grain size distribution ranging from clay to fine sand characterized by EM1 and EM3 (Figs. 6 and 7). The grain size data indicate an environment dominated by fine-grained deposition with periodic higher energy events capable of delivering coarser material. Our analysis of lithology and XRF profiles from cores throughout the lake reveals that this unit can be traced across all four Nedre Midsommersø basins (Fig. 9). We interpret this lithologic unit as reflecting a period when turbid meltwater, characterized by periodic high flow rates, was delivered to Midsommersø. Turbid waters also explain the high sedimentation rates and the low organic carbon concentrations and prevented diatoms from colonizing the lake throughout this interval. From at least 8.2 cal ka BP, and likely earlier, meltwater would have been delivered to Midsommersø from the GrIS, Hans Tausen Ice Cap,

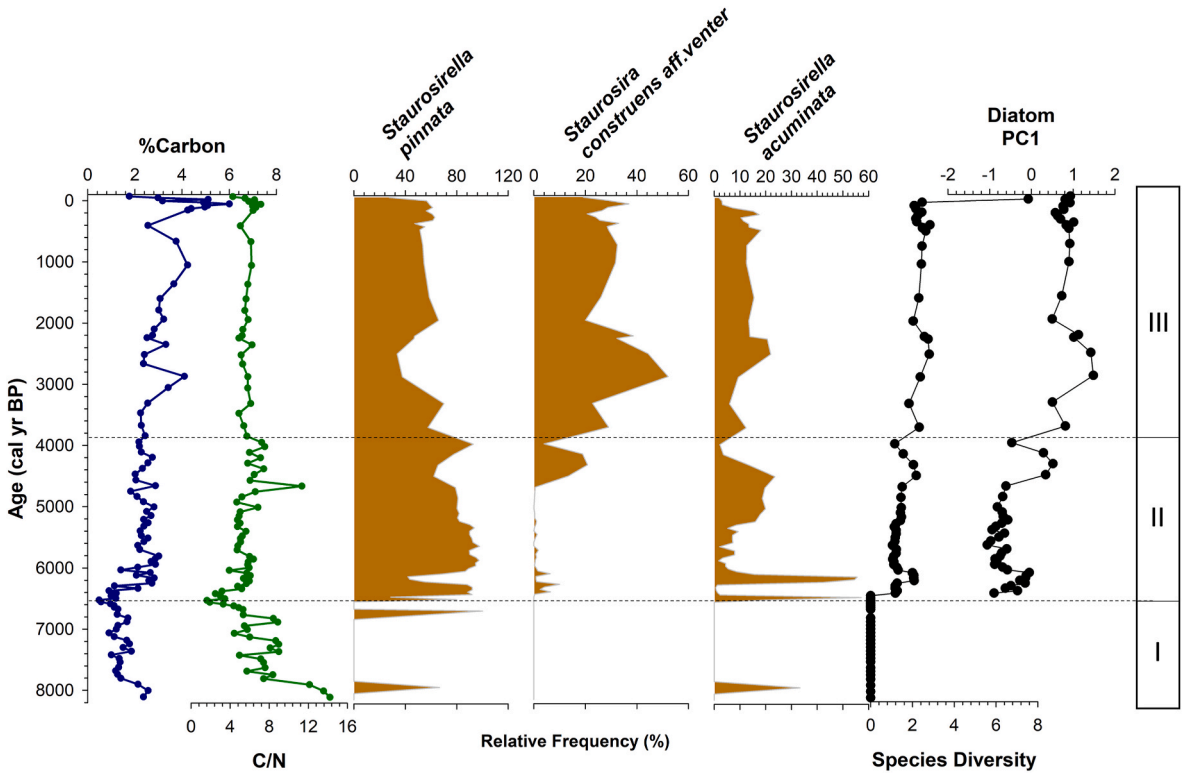

Fig. 8. Total carbon, total carbon to nitrogen ratio (C/N), and diatom assemblage data for core NMD-22-01 and NMP-22-02.

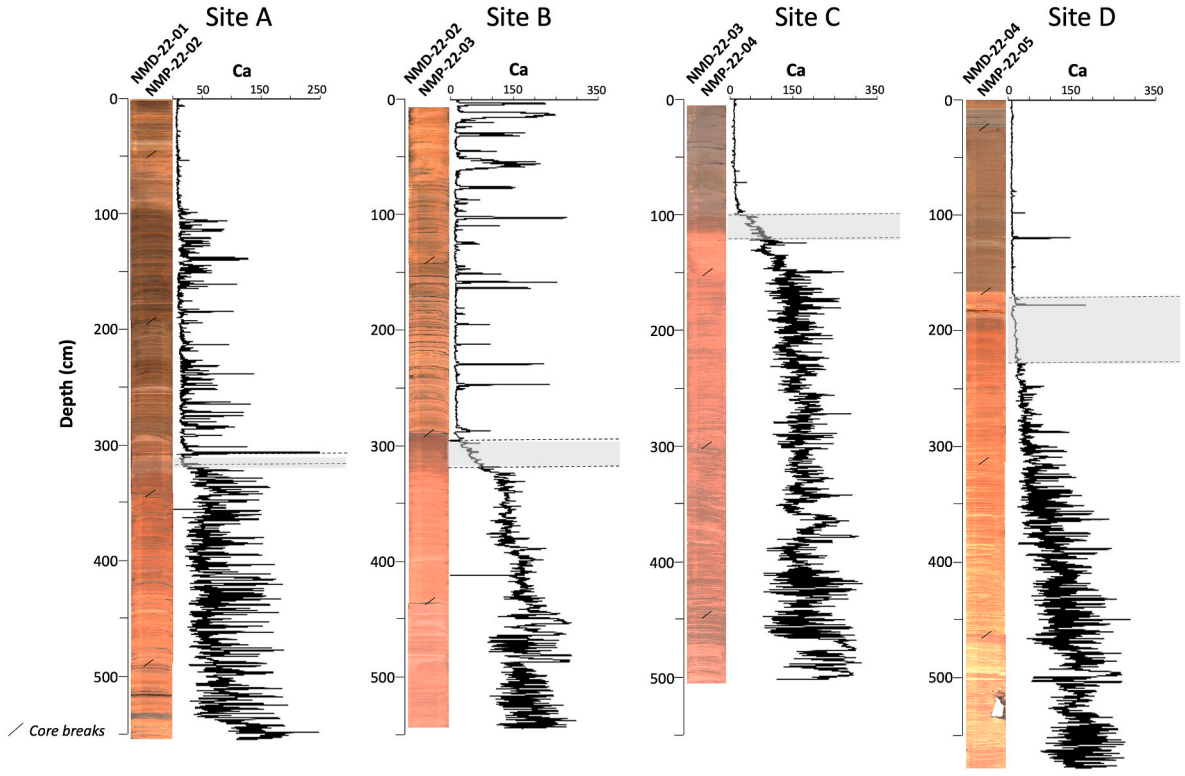

Fig. 9. Core images and scanning XRF Ca profiles for sediment cores recovered from Nedre Midsommersø (Table 1; Fig. 1). The transition in sediment characteristics and Ca values found in each core is highlighted with gray bars.

Bure Ice Cap, and Storm Ice Cap as they retreated into the upper reaches of the watershed. These depositional conditions abruptly ended c. 6.5 cal ka BP when sediment became less dense, more organic rich, and diatom-bearing, all of which we interpret to represent a reduction in glacial meltwater input to Midsommersø. The rapid nature of this transition could indicate: (i) a significant change in GrIS meltwater

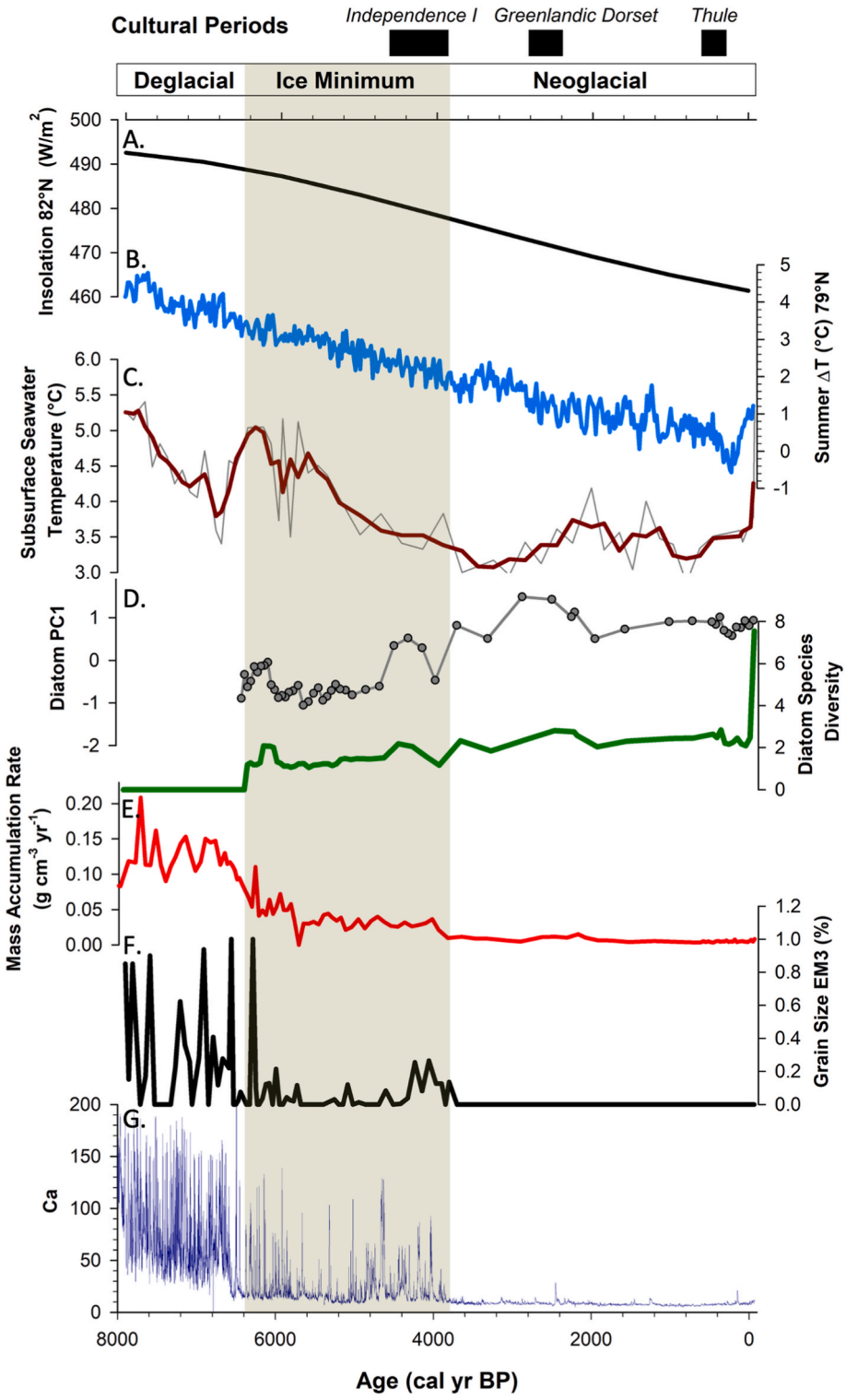

Fig. 10. Comparison of regional records to trends in data from Nedre Misommersø (NM) highlighting changes associated with transitions from deglacial, reduced ice extent during the mid-Holocene, and Neoglacial intervals. (A.) Insolation values at 82°N (Laskar et al., 2004). (B.) Summer (JJA) temperature anomalies at 79°N (Buizert et al., 2018). (C.) Subsurface water temperatures from Fram Strait (Werner et al., 2016). (D.) Diatom data from NM including the PC1 axis and diatom species diversity. (E.) NM mass accumulation rates. (F.) NM grain size trends based on the third end-member 3 (EM3) scores (Fig. 7). (G.) NM scanning XRF Ca profile. Also shown are the approximate intervals of early human settlement of Wandel Dal (Grønnow and Jensen, 2003).

routing as ice retreated up valley, (ii) that the Hans Tausen Ice Cap was a dominant contributor of meltwater and completely melted at c. 6.5 cal ka BP, or (iii) a rapid stabilization of the catchment reducing the suspended sediment load.

Mapping by Leger et al. (2024) generally supports our interpretations of the timing of deglaciation of Nedre Midsommersø. However, they show ice margins up-valley of Midsommersø may have reached their present extent c. 7.5-7.0 cal ka BP, while sedimentation in Nedre Midsommersø shows that intense meltwater input lasted until 6.5 cal ka BP, providing evidence for continued ice retreat. This meltwater

may have derived from continued melt of the southern sector of the Hans Tausen Ice Cap, which modeling suggests did not become ice-free until c. 6.5 cal ka BP (Zekollari et al., 2017), and/or it may have been from continued melting of the sector of the GrIS in the Midsommersø watershed inland from its current position that resulted in rerouting of meltwater. There is evidence from around the GrIS, including data from northwest Greenland (Funder, 1982; Bennike and Weidick, 2001) that in places the margin had retreated within its present-day extent (Briner et al., 2016).

5.2. Reduced ice extent in Wandel Dal: c. 6.5 – 3.9 cal ka BP

At c. 6.5 cal ka BP in Nedre Midsommersø, there was an abrupt change in sedimentation representing a shift to different environmental conditions that persisted until 3.9 cal ka BP (Unit II). This transition is characterized by a sharp decrease in sediment accumulation rate and dry bulk density, accompanied by an increase in organic carbon concentration and the emergence of diatoms (Figs. 2 and 8). Ca values decrease and only display discrete peaks throughout this unit corresponding to coarser sediment layers (Fig. 4). Lithogenic sediment is dominated by silt-sized particles with only periodic fine sand layers occurring throughout this interval as defined by EM3 (Fig. 7). We interpret these characteristics to represent a cessation of meltwater input and reduced ice extent in the catchment from c. 6.5 until 3.9 cal ka BP. These conditions would have decreased overall sedimentation rates and allowed for an increase in lake water clarity that promoted primary productivity and the colonization of the lake by diatoms, which are dominated by benthic taxa typical of large seasonally ice-covered lakes. The periodic input of coarser sediment with high Ca values represents occasional runoff events into the basin, likely associated with spring melt.

Records from around Greenland indicate maximum warmth in the early to middle Holocene (c. 10-5 cal ka BP; Briner et al., 2016; Axford et al., 2021). This timing is similar to trends in Greenland-wide temperature reconstructions (c. 10-6 cal ka BP; Buizert et al., 2018) and the timing of warmer subsurface ocean temperatures in Fram Strait (c. 10.6-5 cal ka BP; Werner et al., 2016), all of which generally lag the peak in local summer insolation (c. 12-10 cal ka BP; Laskar et al., 2004) (Fig. 10). Evidence of warmer early to mid-Holocene conditions is found throughout northern Greenland. In Jørgen Brønlund Fjord, warmer conditions are supported by dates on driftwood, which suggest that the fjords were seasonally ice-free c. 6.7-2.5 cal ka BP (Bennike, 1987; Landvik et al., 2001). The eastern margin of Flade Isblink, 350 km east of Wandel Dal, was smaller than present c. 9.4-4.1 cal ka BP (Hjort, 1997) and mass loss of the ice cap's outlet glaciers began c. 9.4 cal ka BP (Larsen et al., 2019). Southeast of our study area, chironomid assemblage date from two lakes in Store Koldewey, an island off northeast Greenland, indicate greatest temperatures and nutrient availability c. 8-5 cal ka BP (Schmidt et al., 2011) and paleoecological data from a lake in the Skallingen area indicate maximum warmth c. 7.7-4.4 cal ka BP (Wagner and Bennike, 2015). Despite significant regional variations in the timing of the Holocene Thermal Maximum, which is due to local climate and ice conditions, the peak in temperatures generally precedes the interval of reduced ice extent that we interpret in Wandel Dal from c. 6.5-3.9 cal ka BP.

Our interpretation of reduced ice extent relative to modern conditions in Wandel Dal c. 6.5-3.9 cal ka BP, is consistent with evidence for changes in the size of the Hans Tausen Ice Cap during the mid-Holocene. Zekollari et al. (2017) show in their model that the southern margin of the ice cap was ice-free c. 6.5 cal ka BP and that the buildup of ice in this sector did not commence until c. 4.0 cal ka BP. This timing of ice growth is supported by age estimates of 4.0-3.5 cal ka BP on the oldest ice from a core taken at the present-day central dome of the ice cap (Hammer et al., 2001; Madsen and Thorsteinsson, 2001). The absence of ice in southern sector of the Hans Tausen Ice Cap c. 6.5-3.5 cal ka BP suggests that the smaller Bure and Storm Ice Caps were also likely ice free during this interval, and others have shown that the GrIS was at a minimum extent c. 7-4.5 cal ka BP (Larsen et al., 2015; Briner et al., 2016). Taken together, this evidence indicates that the deterioration of the GrIS, which began sometime in the early Holocene, reached its culmination with retreat within its current extent in Wandel Dal and the disappearance of the local ice caps during the interval 6.5-3.9 cal ka BP.

5.3. Neoglacial: c. 3.9 cal ka BP – present

The termination of mid-Holocene conditions in Nedre Midsommersø is marked by an abrupt decrease in sedimentation rate and sediment density, as well as a slight increase in organic carbon content and shift in diatom species (Figs. 2 and 8). This interval is also characterized by finer lithogenic sediment input and a complete absence of coarse sediment, as reflected in the grain size data and persistently low Ca values (Figs. 4 and 7). We interpret these results to indicate a shift to colder and drier conditions, which would have been associated with more extended periods of lake ice cover, enhancing organic matter preservation and reducing snowmelt runoff, thereby restricting the delivery of coarser sediment to the lake.

Climate cooling of the late Neoglacial period is associated with the advance of the GrIS as well as mountain glaciers and ice caps after c. 5-4 cal ka BP in response to declining insolation and regional temperatures (Briner et al., 2016; Kjær et al., 2022). The late Holocene in Wandel Dal is associated with the buildup of the southern sector of the Hans Tausen Ice Cap beginning c. 4-3.5 cal ka BP (Madsen and Thorsteinsson, 2001; Zekollari et al., 2017), and likely the GrIS and Bure and Storm Ice Caps. Despite this ice growth in the Midsommersø catchment, we see decreased sedimentation rates and only a minor shift in grain size characteristics. This evidence reflects the growth of mostly cold-based ice and the limited precipitation in the region, which accumulated on the uplands, resulting in limited runoff.

Distinct glacial advances during the Neoglacial have been recorded in other parts of Greenland (e.g. Balascio et al., 2015; Kjær et al., 2022). The analysis by Kjær et al. (2022) of records from around Greenland found early Neoglacial advances c. 2.5-1.7 cal ka BP and 1.25-0.95 cal ka BP, culminating in advances during the Little Ice Age (LIA), 700-50 yrs. In Midsommersø, we observe no significant changes in sedimentation over the last 3.9 cal ka BP, possibly because the overall cold and dry conditions throughout the late Holocene, combined with the presence of cold-based ice in the catchment, which did not yield a sedimentary signature in this proglacial lake setting. Diatom data also indicate a persistent ice-dominated lake across this interval and up until the last c. 50 years when greater species diversity and habitats became established (Fig. 8). Diatom changes since 1980 CE in Nedre Midsommersø are consistent with the dramatic response of circumarctic diatom communities to recent climate warming and the increase in ice-free summer days over the last several decades (Smol et al., 2005), a trend also observed in northernmost Greenland (Perren et al., 2012).

5.4. Paleoclimate context for past Inuit settlement of Wandel Dal

The Holocene climate and deglacial history of Wandel Dal provides additional perspectives on the context for the early human migration and settlement history of the area (Grønnow and Jensen, 2003; Jensen et al., 2017). The west-east corridor from J.P. Koch Fjord to Independence Fjord, via Wandel Dal, formed the eastern gateway to the *Musk Ox Way*, a term coined by the region's pioneering archaeologist Eigil Knuth (1967a,b, 1984). This region has been envisaged as a critical landscape corridor for animal and human migration from Arctic Canada into Greenland (Jensen et al., 2017; Jensen and Gotfredsen, 2022). However, the archaeology suggests that Wandel Dal was not only a gateway, but that it also served as an important inland hunting area for past populations of the region that were otherwise reliant on marine resources. During the late Holocene there were three separate phases of human settlement of Wandel Dal. Archaeological sites within the valley and around Midsommersø are associated with the Independence I (c. 4.5-3.9

cal ka BP), Greenlandic Dorset (c. 2.8-2.4 cal ka BP), and Thule (c. 1400 CE) cultures (Grønnow and Jensen, 2003) (Fig. 10).

The reconstruction from Nedre Midsommersø provides the first local paleoenvironmental record to provide new context for the migration and settlement history of the Independence I people into Wandel Dal. Our data show reduced ice extent in Wandel Dal just prior to significant climate cooling c. 3.9 cal ka BP characterize the environmental conditions during the first in-migration of humans to the region. Generally warmer climate conditions and reduced ice extent would have been advantageous to both animal and human populations in the valley. The abrupt termination of this interval and onset of colder and drier environmental conditions c. 3.9 cal ka BP corresponds with some of the youngest Independence I dates in Wandel Dal. Such environmental conditions would have been both disadvantageous to migration and hunting, and may have eventually pushed settlement out of the region altogether. Following this interval there is a lack of sensitivity in our record to more subtle changes in paleoenvironmental conditions until 1980 CE, when evidence for warming is observed. Additional sediment and archaeological analysis will be required to provide the environmental context for the later arrival of the Greenlandic Dorset and Thule people, aside from the fact that they occurred within the colder and drier Neoglacial period.

6. Conclusions

Our analysis of sediment properties from Nedre Midsommersø demonstrates that the record characterizes the Holocene deglaciation and climate history of Wandel Dal. Sedimentological data extend back into the early Holocene, c. 8.2 cal ka BP, and contain three distinct phases defined by physical and biological changes reflected in bulk density, mass accumulation rates, carbon and nitrogen content, grain size, diatom assemblages, and scanning XRF profiles. We interpret these as indicators of variations in glacier meltwater input, snowpack melt, and precipitation, and lake primary productivity. The oldest phase of sedimentation (c. 8.2 – 6.5 cal ka BP) reflects a period when turbid meltwater, characterized by periodic high flow rates, was delivered to Midsommersø from the retreating GrIS, Hans Tausen Ice Cap, Bure Ice Cap, and Storm Ice Cap. At c. 6.5 cal ka BP, there was a significant reduction of meltwater input. We interpret the interval from c. 6.5-3.9 cal ka BP to mark a period when ice extent within the catchment was at a minimum. Another transition at c. 3.9 cal ka BP, marks the onset of Neoglacial conditions and a colder and drier climate that was associated with more extended periods of lake ice cover. An absence of any significant changes in sedimentation over the last 3.9 kyr shows that the lake was likely extensively ice covered and insensitive to any signature of Neoglacial ice advances, including the LIA, likely reflecting the growth of mostly cold-based ice and the limited precipitation in the region. However, a marked change in diatom species diversity and habitats beginning in the last c. 50 years shows the impact of recent climate warming due to an increase in the length of the summer ice-free conditions. Overall, we show the sensitivity of this sector of the GrIS and peripheral glaciers in Wandel Dal to Holocene climate conditions. The paleoclimate intervals defined by the Nedre Midsommersø also provide context for the settlement history of Wandel Dal by past Inuit cultures. Specifically, the record shows that the migration of Independence I people into Wandel Dal occurred near the end of the local HTM when ice extent in the valley was at minimum and just prior to the abrupt onset of Neoglacial conditions.

Author contributions

All authors have approved this version of the manuscript we are submitting for publication. Specific author contributions: NLB led the research and writing of the manuscript. RSB, WJD, BP, CKM and NLB designed the study. Fieldwork and sample collection were conducted by JB, BP, WJD, FL, RSB, and FFL. Sediment core and data analysis were conducted by NLB, JB, BP, ED, FL, RS and ZVD. All authors contributed to the interpretation of the results and the writing of the manuscript.

Declaration of competing interest

The authors declare the following financial interests/personal relationships which may be considered as potential competing interests: Nicholas Balascio reports financial support was provided by National Science Foundation. William D'Andrea reports financial support was provided by National Science Foundation. Raymond Bradley reports financial support was provided by National Science Foundation. Bianca Perren reports financial support was provided by UK Research and Innovation Natural Environment Research Council. Francois Lapointe reports financial support was provided by National Science Foundation. If there are other authors, they declare that they have no known competing financial interests or personal relationships that could have appeared to influence the work reported in this paper.

Acknowledgements

This work was jointly funded by the U.S. National Science Foundation (NSF) and the U.K. Natural Environment Research Council (NERC), including NSF grants OPP-2126047 (N.L.B), OPP-2125994 (R.S.B), OPP-2126212 (W.J.D.), OPP-2402628 (F.L.), and NERC grant NE/W007541/1 (B.P.). Support was also provided by a U.S.-NorwayFulbright Scholar Award and a William & Mary Reves Faculty Fellowship to N.L.B. We thank Hans Lange, Mikkel Myrup, Inaluk Schmidt Jacobsen, Nukannguaq Mathiesen, and Aart Verhage for assistance in the field and personnel at Station Nord and the Villim Research Station for logistical support. Benjamin Robson provided assistance with spatial analysis, and Jan Magne Cederstrøm and Ajit Joshi supported laboratory analyses. We also thank Kathryn Adamson and one anonymous reviewer for comments on an earlier draft.

Data availability

A link to the data and/or code is provided as part of this submission.

References

Adamson, K., Lane, T., Carney, M., Delaney, C., Howden, A., 2022. The imprint of catchment processes on Greenlandic ice cap proglacial lake records: analytical approaches and palaeoenvironmental significance. J. Quat. Sci. 37, 1388–1406.
Antoniades, D., Hamilton, P.B., Douglas, M.S.V., Smol, J.P., 2008. In: Lange-Bertalot, H. (Ed.), Iconographia Diatomologica, Diatoms of North America: the Freshwater Floras of Prince Patrick, Ellef Ringnes and Northern Ellesmere Islands from the Canadian Arctic Archipelago, 17, p. 649. A.R.G. Gantner Verlag K.G., Ruggell.
Axford, Y., de Vernal, A., Osterberg, E.C., 2021. Past warmth and its impacts during the Holocene thermal maximum in Greenland. Annu. Rev. Earth Planet Sci. 49, 279–307.
Bakke, J., Balascio, N.L., van der Bilt, W.G.M., Bradley, R.S., D'Andrea, W.J., Gjerde, M., Ólafsdóttir, S., Røthe, R., De Wet, G., 2018. The island of amsterdamøya: a key site for studying past climate in the arctic archipelago of Svalbard. Quat. Sci. Rev. 183, 157–163.
Balascio, N.L., D'Andrea, W.J., Bradley, R.S., 2015. Glacier response to north Atlantic climate variability during the Holocene. Clim. Past 11, 1587–1598.
Beck, H.L., Bennett, B.G., 2002. Historical overview of atmospheric nuclear weapons testing and estimates of fallout in the continental United States. Health Phys. 82, 591–608.
Bennike, O., 1987. Quaternary geology and biology of the Jørgen Brønlund fjord area, north Greenland. Meddelelser om Grønland. Geoscience 18, 24.
Bennike, O., Björk, S., 2002. Chronology of the last recession of the Greenland Ice sheet. J. Quat. Sci. 17, 211–219.
Bennike, O., Weidick, A., 2001. Late Quaternary history around Nioghalvfjerdsfjorden and Jøkelbugten, north-east Greenland. Boreas 30, 205–227.
Besonen, M.B., Patridge, W., Bradley, R.S., Francus, P., Stoner, J.S., Abbott, M.B., 2008. A record of climate over the last millennium based on varved Lake sediments from the Canadian high arctic. Holocene 18, 169–180.
Bintanja, R., 2018. The impact of arctic warming on increased rainfall. Sci. Rep. 8, 16001.
Blaauw, M., Christen, J.A., 2011. Flexible paleoclimate age-depth models using an autoregressive gamma process. Bayesian Analysis 6, 457–474.
Briner, J.P., McKay, N.P., Axford, Y., Bennike, O., Bradley, R.S., de Vernal, A., Fisher, D., Francus, P., Fréchette, B., Gajewski, K., Jennings, A., Kaufman, D.S., Miller, G.,

Rouston, C., Wagner, B., 2016. Holocene climate change in arctic Canada and Greenland. Quat. Sci. Rev. 147, 340–364.
Briner, J.P., Cuzzone, J.K., Badgeley, J.A., Young, N.E., Steig, E.J., Morlighem, M., Schlegel, N.J., Hakim, G.J., Schaefer, J.M., Johnson, J.V., Lesnek, A.J., Thomas, E.K., Allan, E., Bennike, O., Cluett, A.A., Csatho, B., de Vernal, A., Downs, J., Larour, E., Nowicki, S., 2020. Rate of mass loss from the Greenland Ice sheet will exceed Holocene values this century. Nature 586, 70–74. https://doi.org/10.1038/s41586-020-2742-6.
Buizert, C., Keisling, B.A., Box, J.E., He, F., Carlson, A.E., Sinclair, G., DeConto, R.M., 2018. Greenland-wide seasonal temperatures during the last deglaciation. Geophys. Res. Lett. 45, 1905–1914.
Carrivick, J.L., Boston, C.M., King, O., James, W.H.M., Quincey, D.J., Smith, M.W., et al., 2019. Accelerated volume loss in glacier ablation zones of NE Greenland, little ice age to present. Geophys. Res. Lett. 46, 1476–1484. https://doi.org/10.1029/2018GL081383.
Carrivick, J.L., Boston, C.M., Sutherland, J.L., Pearce, D., Armstrong, H., Bjørk, A., et al., 2023. Mass loss of glaciers and ice caps across Greenland since the Little Ice Age. Geophys. Res. Lett. 50. https://doi.org/10.1029/2023GL103950 e2023GL103950.
Croudace, I.W., Rindby, A., Rothwell, R.G., 2006. ITRAX: description and evaluation of a new multi-function X-ray core scanner. In: Rothwell, R.G. (Ed.), New Techniques in Sediment Core Analysis, 267. Geological Society, London, Special Publications, pp. 51–564.
Dietze, E., Hartmann, K., Diekmann, B., et al., 2012. An end-member algorithm for deciphering modern detrital processes from lake sediments of Lake donggi cona, NE Tibetan Plateau, China. Sediment. Geol. 243–244, 169–180.
Dietze, E., Dietze, M., 2019. Grain-size distribution unmixing using the R package EMMAgeo. E&G Quaternary Science Journal 68, 29–46.
Foged, N., 1955. Diatoms from peary land, north Greenland. Medd om Groenland 128 (7), 1–90.
Francus, P., Asikainen, C., 2001. Sub-sampling unconsolidated sediments: a solution for the preparation of undisturbed thin-sections from clay-rich sediments. J. Paleolimnol. 26, 323–326. https://doi.org/10.1023/A:1017572602692.
Funder, S., 1982. 14C-dating of samples collected during the 1979 expedition to north Greenland. Grønlands Geologiske Undersøgelse Rapport 110, 9–14.
Funder, S., Kjeldsen, K.K., Kjær, K.H., Cofaigh, C.Ó., 2011. In: Ehlers, J., Gibbard, P.L., Hughes, P.D. (Eds.), Developments in Quaternary Science, The Greenland Ice Sheet During the past 300,000 Years: a Review, 15, pp. 699–713, 978-0-444-53447-7.
Grønnow, B., Jensen, J.F., 2003. *The Northernmost Ruins of the Globe.* Meddelelser Om Gronland, Man and Society. Danish Polar Center, Copenhagen, p. 403, 29.
Hammer, C.U., Johnsen, S.J., Clausen, H.B., Dahl-Jensen, D., Gundestrup, N., Steffensen, J.P., 2001. The paleoclimatic record from a 345 m long ice core from the hans tausen ice cap. Meddelelser om Grønland, Geoscience 39, 87–95.
Harris, D., Horwath, W.R., van Kessel, C., 2001. Acid fumigation of soils to remove carbonates prior to total organic carbon or carbon-13 isotopic analysis. Soil Sci. Soc. Am. J. 65, 1853–1856.
Hjort, C., 1997. Glaciation, climate history, changing marine levels and the evolution of the northeast water polynya. J. Mar. Syst. 10, 23–33.
Hörhold, M., Münch, T., Weilbach, S., Kipfstuhl, S., Freitag, J., Sasgen, I., Lohmann, G., Vinther, B., Laeppie, T., 2023. Modern temperatures in central-north Greenland warmest in past millennium. Nature 613, 503–507.
Jensen, J.F., Gotfredsen, A.B., 2022. First people and muskox hunting in northernmost Greenland. Acta Boreal. 39 (1), 24–52. https://doi.org/10.1080/08003831.2022.2061763.
Jensen, J.F., Odgaard, U., Funder, S., Plumet, P., 2017. First people in Greenland. In: Kotlyakov, V.M., Velichko, A.A., Vasil'ev, S.A. (Eds.), Human Colonization of the Arctic: the Interaction Between Early Migration and the Paleoenvironment. Academic Press, Amsterdam, The Netherlands, p. 628, 978-0-12-813532-7.
Khan, S.A., Colgan, W., Neumann, T.A., van den Broeke, M.R., Brunt, K.M., Noël, B., et al., 2022. Accelerating ice loss from peripheral glaciers in north Greenland. Geophys. Res. Lett. 49. https://doi.org/10.1029/2022GL098915 e2022GL098915.
Kjær, K.H., Bjørk, A.A., Kjeldsen, K.K., Hansen, E.S., An- dresen, C.S., Siggaard-Andersen, M.-L., Khan, S.A., Søn- dergaard, A.S., Colgan, W., Schomacker, A., Woodroffe, S., Funder, S., Rouillard, A., Jensen, J.F., Larsen, N.K., 2022. Glacier response to the little ice age during the neoglacial cooling in Greenland. Earth Sci. Rev. 227, 103984. https://doi.org/10.1016/j.earscirev.2022.103984.
Knuth, Eigil, 1967a. Archaeology of the Musk-ox Way. Ecole Practique Des Hautes Études, Contributions Du Centre D'Études Arctiques Et Fenno-Scandinaves No. 5. Paris: Sorbonne.
Knuth, Eigil, 1967b. The ruins of the Musk-ox way. Folk 8–9, 192–209.
Knuth, E., 1984. Reports from the Musk-ox Way. A Compilation of Knuth's Published Articles and Expanded with 14C-dates, Private edition. Copenhagen.
Lamoureux, S.F., 1994. Embedding unfrozen lake sediments for thin section preparation. J. Paleolimnol. 10, 141–146.
Landvik, J.Y., Weidick, A., Hansen, A., 2001. The glacial history of the hans tausen Iskappe and the last glaciation of peary land, north Greenland. Meddelelser om Grønland. Geoscience 39, 27–39.
Lapointe, F., Francus, P., Stoner, J.S., Abbott, M.B., Balascio, N.L., Cook, T.L., Bradley, R. S., Forman, S.L., Besonen, M., St-Onge, G., 2019. Chronology and sedimentology of a new 2.9 ka annually laminated record from south sawtooth Lake, Ellesmere Island. Quat. Sci. Rev. 222, 105875.
Larsen, N.K., Kjær, K.H., Lecavalier, B., Bjørk, A.A., Colding, S., Huybrechts, P., Jakobsen, K.E., Kjeldsen, K.K., Knudsen, K.-L., Odgaard, B.V., Olsen, J., 2015. The response of the southern Greenland ice sheet to the Holocene thermal maximum. Geology 43 (4), 291e294. https://doi.org/10.1130/G36476.1.
Larsen, N.K., Levy, L.B., Strunk, A., Søndergaard, A.S., Olsen, J., Lauridsen, T.L., 2019. Local ice caps in finderup land, north Greenland survived the Holocene thermal maximum. Boreas 48, 551–562.
Larsen, J.L., Søndergaard, A.S., Levy, L.B., Olsen, J., Strunk, A., Bjørk, A.A., Skov, D., 2020. Contrasting modes of deglaciation between fjords and inter-fjord areas in eastern north Greenland. Boreas 49, 905–919. https://doi.org/10.1111/bor.12475. ISSN0300-9483.
Laskar, J., Robutel, P., Joutel, F., Gastineau, M., Correia, A.C.M., Levrard, B., 2004. A long term numerical solution for the insolation quantities of the Earth. Astron. Astrophys. 428, 261–285.
Leger, T.P., Clark, C.D., Huynh, C., Jones, S., Ely, J.C., Bradley, S.L., Diemont, C., Hughes, A.L., 2024. A Greenland-wide empirical reconstruction of paleo ice-sheet retreat informed by ice extent markers: PaleoGrIS version 1.0. Clim. Past 20, 701–755.
Macumber, A.L., Patterson, R.T., Galloway, J.M., Falck, H., Swindles, G.T., 2018. Reconstruction of Holocene hydroclimatic vari- ability in subarctic treeline lakes using lake sediment grain-size end-members. Holocene 28, 845–857.
Madsen, K.N., Thorsteinsson, T., 2001. Textures, fabrics and meltlayer stratigraphy in the hans tausen ice core, north Greenland - indications of late Holocene ice cap generation? Meddelelser om Grønland Geoscience 39, 97–114.
Mattingly, K.S., Turton, J.V., Wille, J.D., Noël, B., Fettweis, X., Rennermalm, Å.K., Mote, T.L., 2023. Increasing extreme melt in northeast Greenland linked to foehn winds and atmospheric rivers. Nat. Commun. 14, 1741.
Meyers, P.A., 2003. Applications of organic geochemistry to paleolimnological reconstructions: a summary of examples from the Laurentian Great Lakes. Org. Geochem. 34, 261–289.
Müller, J., Werner, K., Stein, R., Fahl, K., Moros, M., Jansen, E., 2012. Holocene cooling culminates in sea ice oscillations in fram strait. Quat. Sci. Rev. 47, 1–14.
Otosaka, I.N., Shepherd, A., Ivins, E.R., Schlegel, N.-J., Amory, C., van den Broeke, M.R., Horwath, M., Joughin, I., King, M.D., Krinner, G., Nowicki, S., Payne, A.J., Rignot, E., Scambos, T., Simon, K.M., Smith, B.E., Sørensen, L.S., Velicogna, I., White- house, P.L., A, G., Agosta, C., Ahlstrøm, A.P., Blazquez, A., Colgan, W., Engdahl, M.E., Fettweis, X., Forsberg, R., Gallée, H., Gardner, A., Gilbert, L., Gourmelen, N., Groh, A., Gunter, B.C., Harig, C., Helm, V., Khan, S.A., Kittel, C., Konrad, H., Lan- gen, P.L., Lecavalier, B.S., Liang, C.-C., Loomis, B.D., McMillan, M., Melini, D., Mernild, S.H., Mottram, R., Mouginot, J., Nilsson, J., Noël, B., Pattle, M.E., Peltier, W.R., Pie, N., Roca, M., Sasgen, I., Save, H.V., Seo, K.-W., Scheuchl, B., Schrama, E.J.O., Schröder, L., Simonsen, S.B., Slater, T., Spada, G., Sutterley, T.C., Vishwakarma, B.D., van Wessem, J.M., Wiese, D., van der Wal, W., Wouters, B., 2023. Mass balance of the Green- land and antarctic ice sheets from 1992 to 2020. Earth Syst. Sci. Data 15, 1597–1616. https://doi.org/10.5194/essd-15-1597-2023.
Paterson, G.A., Heslop, D., 2015. New methods for unmixing sediment grain size data. G-cubed 16, 4494–4506.
Pedersen, M., Weng, W.L., Keulen, N., Kokfelt, T.F., 2013. A New Seamless Digital 1:500 000 Scale Geological Map of Greenland, 28. Geological Survey of Denmark and Greenland Bulletin, pp. 65–68.
Perren, B.B., Bradley, R.S., Francus, P., 2003. Rapid lacustrine response to recent high arctic warming: a diatom record from sawtooth Lake, ellesmere island, Nunavut. Arctic Antarct. Alpine Res. 35, 271–278.
Perren, B.B., Wolfe, A.P., Cooke, C.A., Kjaer, K.H., Mazzucchi, D., Steig, E.J., 2012. Twentieth century warming revives the world's northernmost lake. Geology 40, 1003–1006.
Post, E., Forchhammer, M.C., Bret-Harte, M.S., Callaghan, T.V., Christensen, T.R., Elberling, B., Fox, A.D., Gilg, O., Hik, D.S., Høye, T.T., Ims, R.A., Jeppesen, E., Klein, D.R., Madsen, J., McGuire, A.D., Rysgaard, S., Schindler, D.E., Stirling, I., Tamstorf, M.P., Tyler, N.J.C., Van Der Wal, R., Welker, J., Wookey, P.A., Schmidt, N. M., Aastrup, P., 2009. Ecological dynamics across the arctic associated with recent climate change. Science 325, 1355–1358.
Reimer, P.J., Austin, W.E.N., Bard, E., et al., 2020. The IntCal20 North- ern Hemisphere radiocarbon age calibration curve (0–55 cal kBP). Radiocarbon 62 (4), 725–757.
Renberg, I., 1990. A procedure for preparing large sets of diatom slides from sediment cores. J. Paleolimnol. 4, 87–90.
Ribeiro, S., Limoges, A., Massé, G., et al., 2021. Vulnerability of the north water ecosystem to climate change. Nat. Commun. 12, 4475.
Ritchie, J.C., McHenry, R.J., 1990. Application of radioactive fallout Cesium-137 for measuring soil erosion and sediment accumulation rates and patterns: a review. J. Environ. Qual. 19, 215–233.
Schmidt, S., Wagner, B., Heiri, O., Klug, M., Bennike, O., Melles, M., 2011. Chironomids as indicators of the Holocene climatic and environmental history of two Lakes in northeast Greenland. Boreas 40, 116–130. https://doi.org/10.1111/j.1502-3885.2010.00173.x. ISSN 0300-9483.
Smol, J.P., Wolfe, A.P., Birks, H.J.B., Douglas, M.S.V., Jones, V.J., Korhola, A., Pienitz, R., Rühland, K., Sorvari, S., Antoniades, D., Brooks, S.J., Fallu, M.-A., Hughes, M., Keatley, B.E., Laing, T.E., Michelutti, N., Nazarova, L., Nyman, M., Paterson, A.M., Perren, B., Quinlan, R., Rautio, M., Saulnier-Talbot, E., Siitonen, S., Solovieva, N., Weckström, J., 2005. Climate-driven regime shifts in the biological communities of arctic lakes. Proceedings of the National Academy of Sciences of the United States of America 102, 4397–4402.
Taylor, P.C., Boeke, R.C., Boisvert, L.N., Feldl, N., Henry, M., Huang, Y., Langen, P.L., Liu, W., Pithan, F., Sejas, S.A., Tan, I., 2022. Process drivers, inter-model spread, and the path forward: a review of amplified arctic warming. Front. Earth Sci. 9, 758361.
Wagner, B., Bennike, O., 2015. Holocene environmental change in the Skallingen area, eastern north Greenland, based on a lacustrine record. Boreas 44, 45–59.
Weltje, G.J., 1997. End-member modeling of compositional data: numerical-statistical algorithms for solving the explicit mixing problem. Math. Geol. 29, 503–549.

Werner, K., Spielhagen, R.F., Bauch, D., Hass, H.C., Kandiano, E., 2013. Atlantic water advection versus sea-ice advances in the eastern fram strait during the last 9 ka: multiproxy evidence for a two-phase Holocene. Paleoceanogr. Paleoclimatol. 28, 283–295.

Werner, K., Müller, J., Husum, K., Spielhagen, R.F., Kandiano, E.S., Polyak, L., 2016. Holocene sea subsurface and surface water masses in the fram strait – comparisons of temperature and sea-ice reconstructions. Quat. Sci. Rev. 147, 194–209.

Zekollari, H., Lecavalier, B.S., Huybrechts, P., 2017. Holocene evolution of hans tausen Iskappe (Greenland) and implications for the palaeoclimatic evolution of the high arctic. Quat. Sci. Rev. 168, 182–193.